



Physico-mechanical properties of loess-paleosol sequence from Q₄ to Q₁ strata in the Chinese Loess Plateau

Jianghong Zhu¹ · Huyuan Zhang^{1,2} · Shengqing Yang¹ · Tingting Wang¹ · Guangping Zhou¹

Received: 16 March 2021 / Accepted: 25 August 2022 / Published online: 14 September 2022
© Springer-Verlag GmbH Germany, part of Springer Nature 2022

Abstract

With the rapid development of the Chinese Loess Plateau, engineering projects built in the deep loess strata may be concurrently constructed in the Q₄, Q₃, Q₂, and Q₁ strata from top to bottom. However, the physico-mechanical properties of the loess-paleosol sequence from Q₄ to Q₁ strata have been unclear. In this paper, the physico-mechanical properties of the loess-paleosol sequence in the Zaosheng profile of Eastern Gansu were determined, and the relationship between chemical properties, microstructures, and physico-mechanical properties was discussed. The results showed that the dry density, specific gravity, saturation, liquid limit, compressive modulus, characteristic value of foundation bearing capacity, and cohesion of loess and paleosol exhibited an overall increasing trend from Q₄ to Q₁ strata, and their values tended to fluctuate regularly with depth. These parameters of the paleosol were larger than those of the underlying loess, while the fluctuation pattern between the internal friction angle and depth was opposite to the above. The fluctuation pattern of water content from Q₄ to Q₁ strata was bounded by the groundwater level. Moreover, the increase in chemical weathering intensity from northwest to southeast Loess Plateau would, therefore, contribute to lower (higher) clay content, liquid limit, and plastic index of the loess and paleosol in Q₄ to Q₁ strata in the northwest (southeast), and decreasing sand content in the corresponding direction.

Keywords Loess-paleosol sequence · Physico-mechanical properties · Strata distribution · Chemical properties · Microstructure · Chinese Loess Plateau

Introduction

Loess is an aeolian sediment deposited under arid and semi-arid conditions in the Quaternary period. It has a porous and weakly cemented microstructure with poor engineering properties, which is closely related to human activity and environmental development (Zhang 1980; Karl 2001; Zhuang et al. 2018). Paleosol is the soil formed in the warm periods during the long-term accumulation of loess (Sylvain et al. 1996; Björn et al. 2011; Huang et al. 2018). The Chinese Loess Plateau is the area with the thickest continuous distribution of loess strata in the world (Fig. 1). Loess and

paleosol are the basic stratigraphic units of the loess strata, which are divided into Q₄, Q₃, Q₂, and Q₁ strata from top to bottom (Liu 1985). The related geological disasters often occur in groups, causing serious environmental damage to the neighboring areas.

The past few decades have witnessed the advancement of engineering construction in the Loess Plateau, including the high-speed railways, highways, and deep foundations of high-rise buildings constructed in deep loess strata (Zhu et al. 2021). The interaction between the deep loess strata and engineering has a non-negligible impact on the geological environment of the Loess Plateau, which may aggravate the risk of geological disasters (Sun et al. 2016; Li et al. 2019; Xue et al. 2019). The physico-mechanical properties of the loess-paleosol sequence from Q₄ to Q₁ strata are the important basis for analyzing the stability of projects built in deep loess strata, which need to be studied urgently.

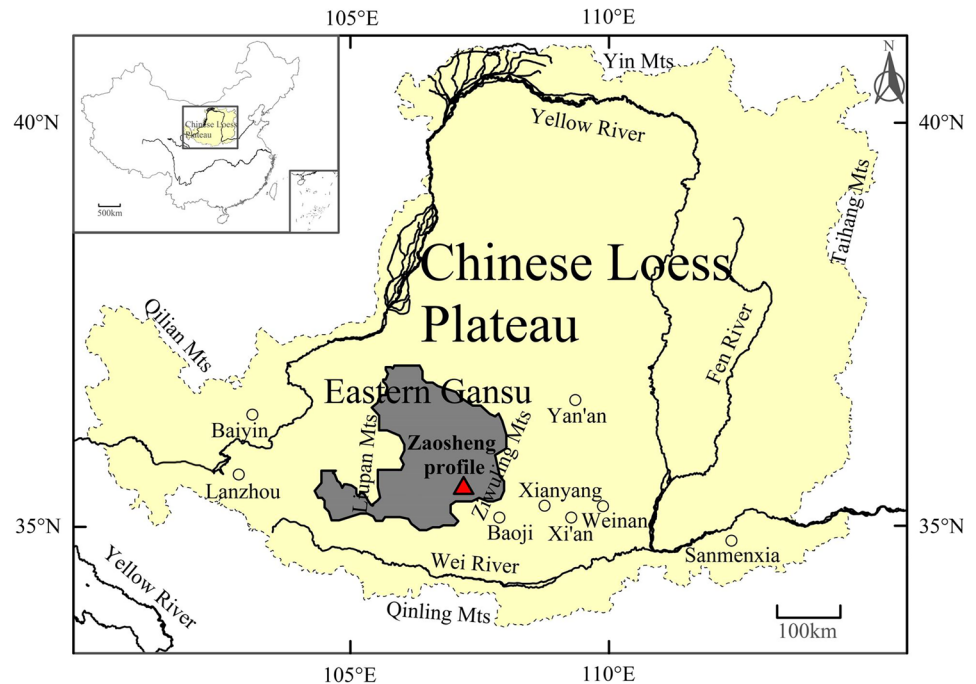
In recent years, extensive investigations on the physico-mechanical properties of loess have been conducted. Metelková et al. (2012) investigated the long-term variations in the pore structure of Q₃ loess treated with 1–8% of lime (CaO). Pei

✉ Huyuan Zhang
zhanghuyuan@lzu.edu.cn

¹ College of Civil Engineering and Mechanics, Lanzhou University, Rd 222 South Tianshui, Lanzhou, Gansu 730000, China

² Key Laboratory of Mechanics On Disaster and Environment in Western China (Lanzhou University), Ministry of Education, Lanzhou 730000, China

Fig. 1 Location of the research area in the Loess Plateau



et al. (2015) analyzed the physical properties of Q_3 loess modified by adding lime and fly ash piles after curing for 28 days. Zhang et al. (2018) determined the variations in the physical and chemical properties of Q_3 loess at laboratory temperatures ranging from 20 to 1000 °C. Li et al. (2020b) adopted a multi-temporal high-resolution digital elevation model to study the temporal and spatial patterns of erosion in the Q_4 loess and Q_3 loess in the cutting slope. The studies on the physical and mechanical properties of loess have mainly focused on the Q_4 loess and Q_3 loess located in the surface of the deep loess strata, while little attention has been paid to the physico-mechanical properties of the Q_2 loess and Q_1 loess in the middle and bottom of the deep loess strata.

At present, the properties of paleosol have also been widely investigated. Chen et al. (1999) measured the Rb, Sr, and magnetic susceptibility of paleosol from the Lochuan profile and Huanxian profile in China. Jahn et al. (2001) analyzed the chemical and Nd–Sr isotopic compositions of paleosol from Xining and Qingyang in the Loess Plateau, to understand the paleoclimate variations during the last 140 ka. Zhang et al. (2013) investigated the element compositions of the loess-paleosol sequence in the Ili Basin and found that the loess and paleosol are in the degrees of weak chemical weathering. Li et al. (2020a) determined the geochemical compositions of paleosol in the western Sichuan Basin and identified the factors of paleoclimate variations in the Sichuan Basin. Though these studies have mainly focused on the chemical properties of paleosol, the physico-mechanical properties of paleosol have been poorly explored, and little research has been done on the physico-mechanical properties

of the loess-paleosol sequence from Q_4 to Q_1 strata in the whole deep loess strata.

With the rapid development of the Loess Plateau, growing numbers of engineering projects are likely to be built, overlapping in the Q_4 , Q_3 , Q_2 , and Q_1 strata of the deep loess strata. The knowledge of the environment in the Loess Plateau should not be limited to the physico-mechanical properties of the Q_4 and Q_3 loess in the surface of the deep loess strata, and more efforts should be paid to the physico-mechanical properties of the loess-paleosol sequence from Q_4 to Q_1 strata in the whole deep loess strata. The relationship between the physico-mechanical of loess and those of paleosol should also be explored and determined. Therefore, in the study, we focused on the profile of the loess tableland in Eastern Gansu to analyze the longitudinal distribution of the physico-mechanical properties of the loess-paleosol sequence from Q_4 to Q_1 strata. The relationship between the chemical properties, microstructures, and physico-mechanical properties was discussed to explore the underlying mechanisms for the variations in the physical–mechanical properties. Meanwhile, the distribution of chemical and physical properties of loess-paleosol sequences in the Loess Plateau was determined by comparing the physical and chemical properties in multiple places. The results provide insightful understandings of the properties of the deep loess strata, and basic parameters of engineering geological conditions for the construction of the deep loess strata, and can serve as a theoretical basis for the protection of the geological environment in the Loess Plateau.

Research areas and methods

Research areas

Loess tableland is a typical landform of the Loess Plateau. It is characterized by a flat and wide top surface with an inclination of less than 1° over the central part, surrounded by deep gullies. The strong retrogressive erosion over the gully heads makes the petal-like loess tableland in plain view (Liu 1985; Xiong et al. 2014).

In this study, the profile of the loess tableland in Eastern Gansu was selected as the research object. The Loess Plateau in Eastern Gansu Province covers Qingyang and Pingliang City (Fig. 1). It extends to Ziwuling Mountains in the east, the Jinghe River in the south, Liupan Mountains in the west, and Baiyu Mountains in the north (Fig. 2). The loess tableland is widely distributed in Eastern Gansu. Among the loess tablelands in Eastern Gansu, the Dongzhi tableland is the largest loess tableland in China, with a tableland surface area of 910 km². And the Zaosheng tableland is the second-largest loess tableland in China, with a tableland surface area of 335 km² (Li et al. 2014; Leng et al. 2018; Guo et al. 2020).

Investigations on strata distribution of loess tablelands in Eastern Gansu

The profile of the on-site investigation is located in the Zaosheng tableland, with an altitude of about 1250 m at the top of the tableland (simply referred to as Zaosheng profile). The Zaosheng tableland is characterized by flat and open surfaces. The surrounding gullies are cut, and the natural profiles at the gullies are exposed. The investigation scopes mainly included natural profiles at gullies and artificially exposed profiles. During the investigation, the lithology, occurrence, and color of the loess strata were recorded (Fig. 3).

In the loess tableland of Eastern Gansu, only the Bajiazui profile, Huoxianggou profile, and Zhengning profile have been studied (Wang and Sadao 1985; Liu et al. 1988; Xi et al. 2018), and little knowledge has been given to the distribution characteristics of the loess strata in the whole tableland. The distribution of loess strata is an important consideration when analyzing the engineering geological conditions of the loess tableland. Thus, this study mainly focused on the Dongzhi tableland and Zaosheng tableland in Eastern Gansu, and determined the distribution characteristics of the loess strata in the Dongzhi tableland and Zaosheng tableland, to provide an engineering geological basis for the analysis of the physico-mechanical properties of the loess-paleosol sequence in the Zaosheng profile.

High-speed railway, oil exploitation, and other major projects were built in the Dongzhi tableland and Zaosheng tableland. The borehole data of Lines A and C in the Dongzhi tableland and Zaosheng tableland were collected from the exploration data of these major projects. The borehole distribution of Line A is shown in Fig. 2b, and the borehole distribution of Line C was uniform, with an interval of 500 m between the two boreholes. Based on the analysis of the loess thickness in the boreholes of the Dongzhi tableland and Zaosheng tableland, and combined with the stratigraphic characteristics of the Zaosheng profile, the distribution characteristics of the loess strata in the Dongzhi tableland and Zaosheng tableland were determined.

Testing of physico-mechanical properties of loess-paleosol sequence

Drilling was carried out from Q₄ to Q₂ strata in the Zaosheng profile, and the samples were taken from the middle of the S₀, L₁, S₁, L₂, S₂, L₃, S₃, L₄, S₄, L₅, S₅, L₆, S₆, L₇, and S₇ layers (Fig. 3). The sample diameter was 142 mm during the drill, and the sample disturbance width is generally considered to be 10 mm (Chang and Zhang 2018). Therefore, the sample of the physico-mechanical properties test (diameter: 61.8 mm), which was taken from the center of the drilled

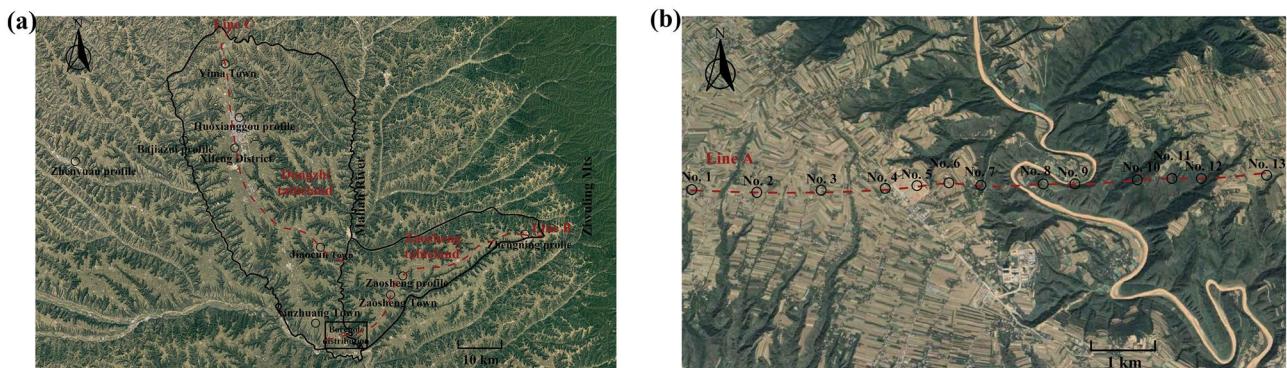


Fig. 2 Loess tablelands in Eastern Gansu **a** Dongzhi tableland and Zaosheng tableland **b** Borehole distribution in Xinzhuang Town


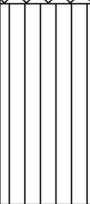


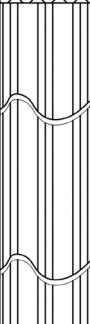
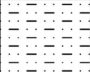
| Serial number | Chronostratigraphy | Stratigraphic name | Columnar section | Ordinal number of layer | Total thickness (m) | Layer thickness (m) | Layer feature |
|---------------|-----------------------------|--------------------------|---|-------------------------|---------------------|---|--|
| 1 | Q ₄ | Potou loess |  | S ₀ | 1.72 | 1.72 | Dark red, well-developed joints and wormholes, with a small amount of white hyphae and a very serious collapsibility. |
| 2 | Q ₃ | Manlan loess |  | L ₁ | 17.11 | 15.39 | Yellow-brown, slightly wet, uniform soil, well-developed wormholes, with a small amount of black spots. |
| 3 | | | | S ₁ | 19.42 | 2.31 | Brown red, slightly wet, uniform soil, well-developed wormholes, with a small amount of white mycelia and less calcareous nodules, the diameter of calcareous nodules is 1.0-2.0 cm. |
| 4 | | | | L ₂ | 31.84 | 12.42 | Yellow-brown, slightly wet, uniform soil, well-developed wormholes, with a small amount of black spots. |
| 5 | Q ₂ ² | Lishi loess (Upper part) |  | S ₂ | 35.52 | 3.68 | Brown red, slightly wet, uniform soil, well-developed wormholes, with a small amount of white mycelia and less calcareous nodules, the diameter of calcareous nodules is 1.0-2.0 cm. |
| 6 | | | | L ₃ | 51.13 | 15.61 | Yellow-brown, slightly wet, uniform soil, well-developed wormholes, with a small amount of black spots. |
| 7 | | | | S ₃ | 56.19 | 5.06 | Red-brown, slightly wet, uniform soil, well-developed wormholes and pinholes, containing a small amount of white hyphae. |
| 8 | | | | L ₄ | 61.81 | 5.62 | Yellow-brown, slightly wet, uniform soil, slightly dense structure, with well-developed joints, wormholes and pinholes. |
| 9 | | | | S ₄ | 65.37 | 3.56 | Red-brown, slightly wet, uniform soil, strong stickiness, well-developed wormholes, containing a small amount of white mycelia and less calcareous nodules. |
| 10 | | | | L ₅ | 68.16 | 2.79 | Yellow-brown, slightly wet, uniform soil, slightly dense structure, with well-developed joints, wormholes and pinholes. |
| 11 | | | | S ₅ | 72.12 | 3.96 | Brown red, slightly wet, uniform soil, containing a small amount of white hyphae. |
| 12 | Q ₂ ¹ | Lishi loess (Under part) |  | L ₆ | 86.28 | 14.16 | Yellow-brown, slightly wet, uniform soil, well-developed joints and pinholes, containing a small amount of white mycelia. Brown red, slightly wet, hard, uniform soil, compact structure, strong stickiness, containing a small amount of white mycelia, less calcareous nodules, and a lot of black spots in the part. |
| 13 | | | | S ₆ | 87.74 | 1.46 | Yellow-brown, slightly wet, hard, uniform soil, compact structure, well-developed joints and pinholes. |
| 14 | | | | L ₇ | 89.96 | 2.22 | Red-brown, slightly wet, hard, uniform soil, compact structure, well-developed pinholes, containing a large number of black spots. |
| 15 | | | | S ₇ | 91.01 | 1.05 | |
| 16 | | | | Q ₁ | Wucheng loess |  | WL |
| 17 | K ₁ | Sandstone |  | K | -- | -- | Different degrees of weathering, wet, soft rock, argillaceous structure, layered structure, with well-developed cracks and a good overall integrity. |

Fig. 3 Zaosheng profile

sample (with a diameter much smaller than 122 mm, i.e., the drilled sample diameter minus twice the disturbance width), could be regarded as undisturbed.

The Q_1 strata are divided into the Q_1^2 and Q_1^1 strata. Compared with Q_4 , Q_3 , and Q_2 loess, Q_1 loess has a compact structure and relatively small variation in engineering geological properties (Xi et al. 2018). Thereby, when the tunnel of the Yinchuan-Xi'an high-speed railway was built in the Q_1 strata near the Zaosheng profile, two samples of loess and paleosol were taken from the Q_1^2 strata, and two samples of loess and paleosol were taken from the Q_1^1 strata. The properties of these four samples represented the property variations of the loess-paleosol sequence in the Q_1 strata. In tunnel excavation, samples were taken after a soil pit deeper than 3 m was excavated at the sampling point with a shovel. All undisturbed samples in the Q_1 strata in this study were taken from the soil layer more than 3 m from the tunnel bottom to ensure that the samples were not disturbed by tunnel excavation and manual excavation.

There were 19 groups of samples in this study. The longitudinal wave velocity is affected by the dry density, water content, and internal structure of soil (Fratta et al. 2005; Zhang et al. 2021). The longitudinal wave velocities of all undisturbed samples were tested prior to the physico-mechanical properties test. Samples in the same group must satisfy the conditions of similar longitudinal wave velocities.

For each group of samples, the Laser Particle Analyzer (Mastersizer 2000, Malvern Instrument Ltd, UK) was used to determine the particle size of the samples (Fig. 4a). Based on the China National Standards GB/T 50123–2019 (Standardization Administration of China (SAC) 2019), the physical properties such as water content, dry density, specific gravity, void ratio, and liquid plastic limit of the samples were tested. In addition, in the construction of loess strata, the collapsibility, shear strength, compressibility, and foundation bearing capacity of the soil are the mechanical properties of major concern (Zhang et al. 2018; Liu et al. 2022; Zhu et al. 2022). Thus, the collapse test, free swell test, direct shear test, consolidation test, and field standard penetration test were carried out on the samples (Fig. 4b–e).

Testing of chemical properties and microstructures of loess-paleosol sequence

To explore the underlying mechanisms for the variations in the physico-mechanical properties of the samples, the chemical properties and microstructures of the samples were tested (Fig. 4f–g). The major element compositions of the samples were analyzed by the X-ray fluorescence spectrometer (Magix pw2403, Panalytical, Netherlands), whereas the X-ray diffraction (PANalytical X'Pert Pro MPD, Panalytical, Netherlands) was utilized to analyze the major mineral compositions of the samples. The diffraction patterns were determined using Co-K α radiation with a Bragg angle (2θ) range of 5–75° under an operating voltage and current of 40 kV and 40 mA, respectively. The microstructures of the samples were observed by the scanning electron microscope (SU-1500, Hitachi, Japan).

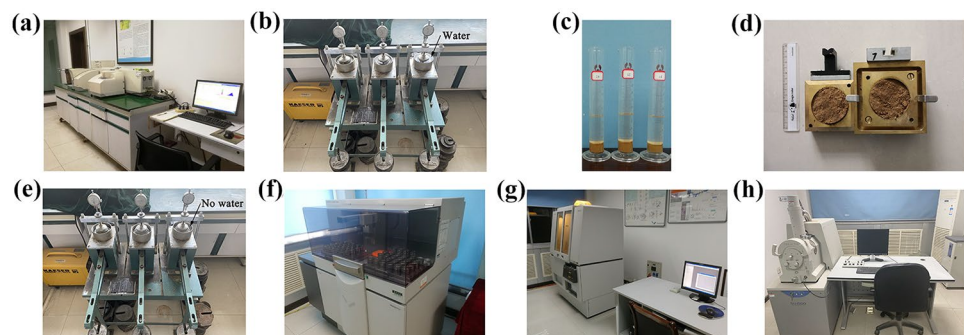
Results

Strata distribution of loess tablelands in Eastern Gansu

Based on the stratigraphic division method (Sun 2005), the boundary positions of the climatic stratigraphic units in the Zaosheng profile were determined by comparing the field measurement results with the Huoxianggou profile (Liu et al. 1988) (Fig. 3). The profile is 247.21 m thick, with a complete sequence from Q_4 to Q_1 strata. In particular, the Q_4 strata are 1.7 m thick, the Q_3 strata are 17.72 m thick, the Q_2 strata are 71.59 m thick, and the Q_1 strata are 156.2 m thick.

To explore the altitude characteristics of the top and bottom of the loess strata in the Zaosheng tableland, the loess strata distribution along Line A in Xinzhuang Town was firstly analyzed (Fig. 5). Then, by comparing the boreholes in Xinzhuang Town, Zaosheng profile, and Zhengning profile (Xi et al. 2018), the loess strata distribution in the east–west direction of the Zaosheng tableland was determined.

Fig. 4 Tests and instruments. **a** Laser Particle Analyzer. **b** Collapse test. **c** Free swell test. **d** Direct shear test. **e** Consolidation test. **f** X-ray fluorescence spectrometer. **g** X-ray diffraction. **h** Scanning electron microscope



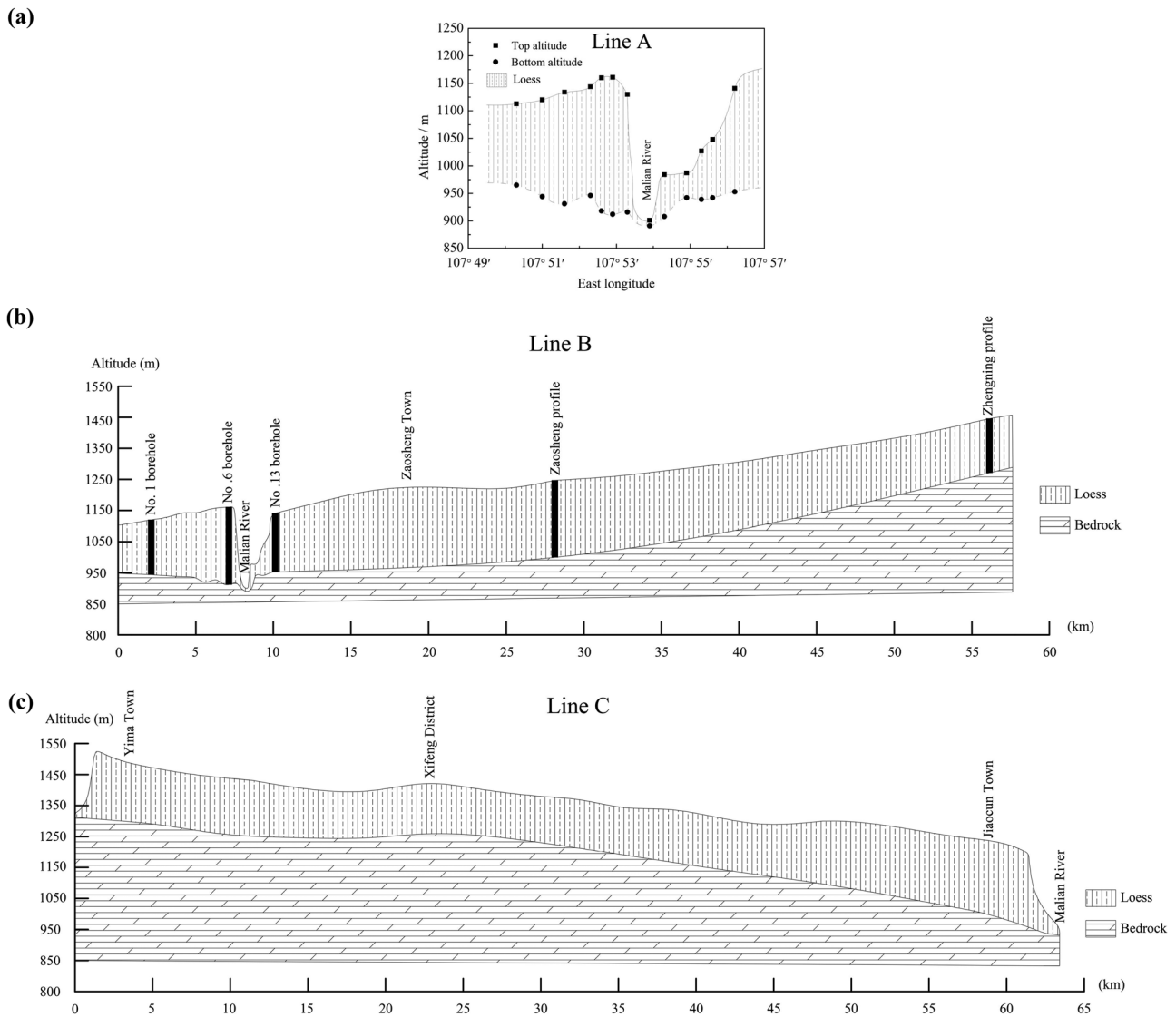


Fig. 5 Loess strata distribution of loess tableland in Eastern Gansu. **a** Xinzhuang town. **b** Zaosheng tableland. **c** Dongzhi tableland

As shown in Fig. 5b, the top altitude of the Malian River is the lowest at about 900 m. From the Malian River eastward to the Zhengning profile, the top altitude gradually rises, and the top altitude of the Zhengning profile is about 1420 m. The variation in the bottom altitude of the loess strata is similar to that in the top altitude. The bottom altitude of the loess strata is about 890 m at the Malian River, and about 1250 m at Ziuling Mountains. However, from the Malian River to the Zhengning profile, the variation in the top altitude of the loess strata is first greater than and then smaller than that in the bottom altitude. Hence, the loess thickness of the Zaosheng tableland increases first and then decreases from west to east. The place with the largest loess thickness is located in Zaosheng Town near the Malian River, and the thickness of the loess strata is

about 260 m. Topographically, the west of Eastern Gansu is Liupan Mountains and the east is Ziuling Mountains (Figs. 1 and 2a), with the top surface of the bedrock at the bottom of the loess strata along the Malian River in the area marking the lowest altitude, while the top surface of the bedrock at both sides of the area has a high altitude. This means that Eastern Gansu is a loess accumulation basin with a huge thickness in paleogeography. Besides, loess is an aeolian sediment deposited under arid and semi-arid conditions in the Quaternary period (Zhang 1980; Karl 2001; Zhuang et al. 2018). It could be deduced that from the Malian River eastward to the Ziuling Mountains or westward to the Liupan Mountains, the top altitude of the bedrock gradually rises and the loess strata tend to become thinner. Thus, in Eastern Gansu, the loess strata near the

Malian River is the thickest from the east–west direction. As shown in Figs. 2a and 6a, from the Zhenyuan profile to the Bajiazui profile (Wang and Sadao 1985), and then to the Huoxianggou profile (Liu et al. 1988), the thickness of the loess strata gradually decreases, which is consistent with the above pattern.

By analyzing the borehole data of Line C, the loess distribution in the north–south direction of the Dongzhi tableland was obtained (Fig. 5c). In the north–south direction,

the thickness of the loess strata in Yima Town in the north of the Dongzhi tableland is about 215 m, while the thickness in Xifeng District (the middle of the Dongzhi tableland) is about 170 m. In Xinzhuang Town and Jiaocun Town (the south of the Dongzhi tableland), the thickness is about 250 m. The thickness of the loess strata in the Dongzhi tableland decreases first and then increases from north to south, and the thickness of the loess strata in the south is greater than that in the north.

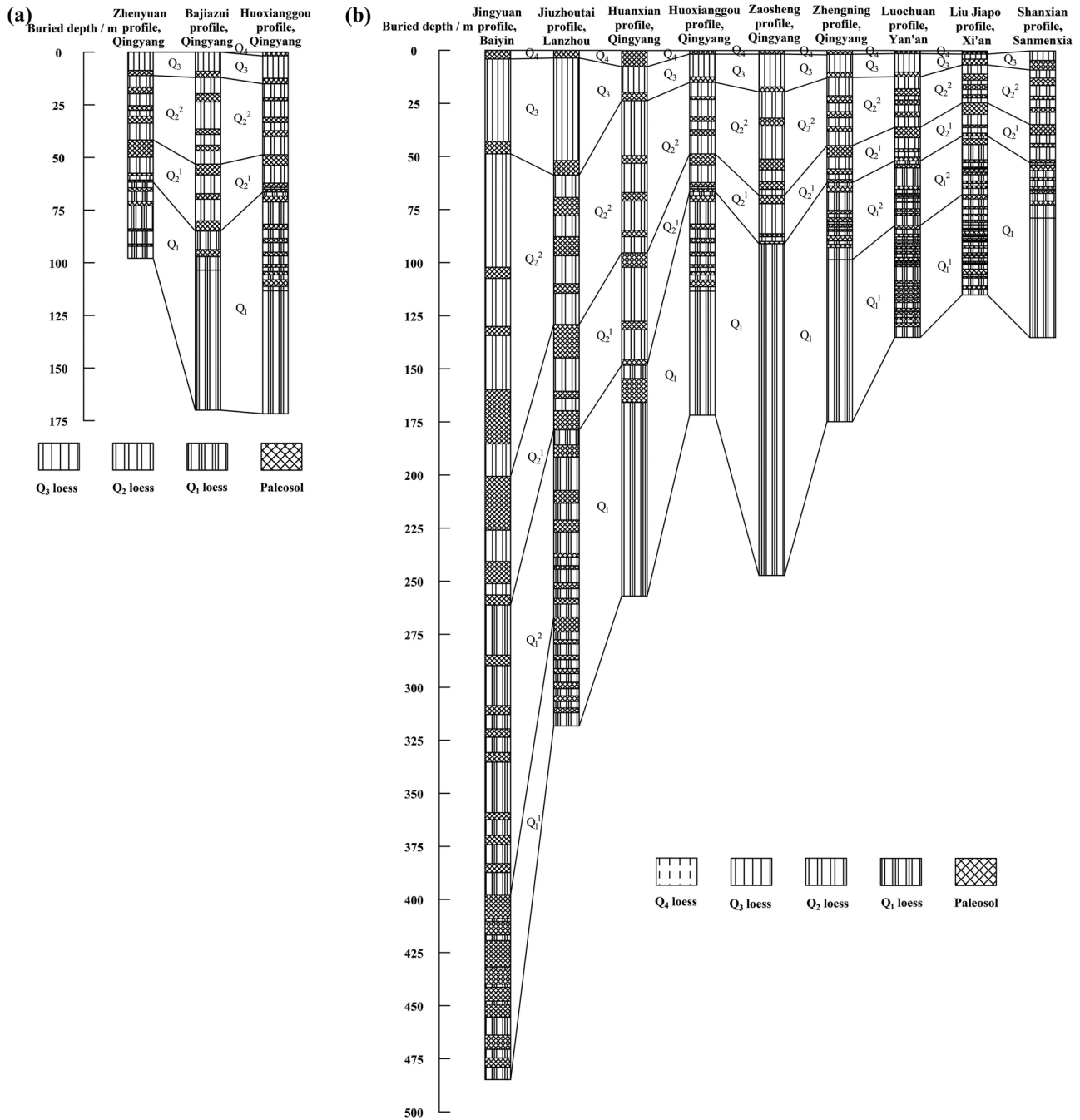


Fig. 6 Loess profiles. a Eastern Gansu. b Loess Plateau

In the Dongzhi tableland and Zaosheng tableland, the thickness of loess strata is 150–260 m. In the Bajiazui profile (Wang and Sadao 1985), the total thickness is 170.0 m, and the thicknesses of the Q_3 , Q_2 , and Q_1 strata are 12.0, 73.0, and 85.0 m, respectively. In the Huoxianggou profile (Liu et al. 1988), the Q_4 strata are 1.3 m thick, the Q_3 strata are 13.3 m thick, the Q_2 strata are 51.4 m thick, and the Q_1 strata are 107.6 m thick, making a total thickness of 173.6 m. In the Zhengning profile (Xi et al. 2018), the thickness of the Q_4 strata is 1.1 m, that of the Q_3 strata is 11.7 m, that of the Q_2 strata is 63.4 m, and that of the Q_1 strata is 98.6 m, with a total thickness of 174.8 m. Moreover, the Zaosheng profile, Bajiazui profile, Huoxianggou profile, and Zhengning profile are far away from each other (Fig. 2a). Zaosheng profile is located near the thickest loess strata in Eastern Gansu. Bajiazui profile and Huoxianggou profile are located near the thinnest loess strata in the Dongzhi tableland, and Zhengning profile is located near the thinnest loess strata in the Zaosheng tableland. Therefore, it could be judged that in the Dongzhi tableland and Zaosheng tableland, the Q_4 strata are 0–2 m thick, the Q_3 strata are 10–20 m thick, the Q_2 strata are 50–80 m thick, the Q_1 strata are 90–160 m thick, and the total thickness is 150–260 m.

The profiles of the loess tablelands in Eastern Gansu were compared with the typical profiles of the Loess Plateau (Wang and Sadao 1985; Liu et al. 1988; Bronger and Heinkele 1989; McIntosh et al. 1996; Sun 2005; Xue et al. 2006; Xi et al. 2018). In Fig. 6b, the profiles are arranged from left to right, representing the northwest to the southeast of the Loess Plateau. The thickness distribution of the loess strata in Eastern Gansu is related to the topography of the bedrock, and the loess thickness of the Zaosheng profile is larger than that of the Huoxianggou profile. However, in general, the thickness of the loess strata gradually decreases from northwest to southeast in the Loess Plateau.

From the above analysis, in the east–west direction of the loess tableland in Eastern Gansu, the loess strata near the Malian River should be the thickest. The Zaosheng profile in this study is located near the Malian River, with a larger thickness (247.21 m). The loess-paleosol sequence distribution should be the most complete in the loess tableland of Eastern Gansu, and its thickness is consistent with the loess distribution characteristics of the whole Loess Plateau. Thereby, the Zaosheng profile in this study is representative.

Physical properties of loess-paleosol sequence

In loess, the silt ranged from 77.26 to 87.21%, while the variation range of clay was 5.45–9.80%, and that of sand was 4.17–14.98% (Fig. 7). In paleosol, the variation ranges of silt, clay, and sand were 79.37–88.35%, 5.38–13.00%, and 2.27–12.87%, respectively. From Q_4 to Q_1 strata, the clay and silt contents of loess and paleosol tended to increase,

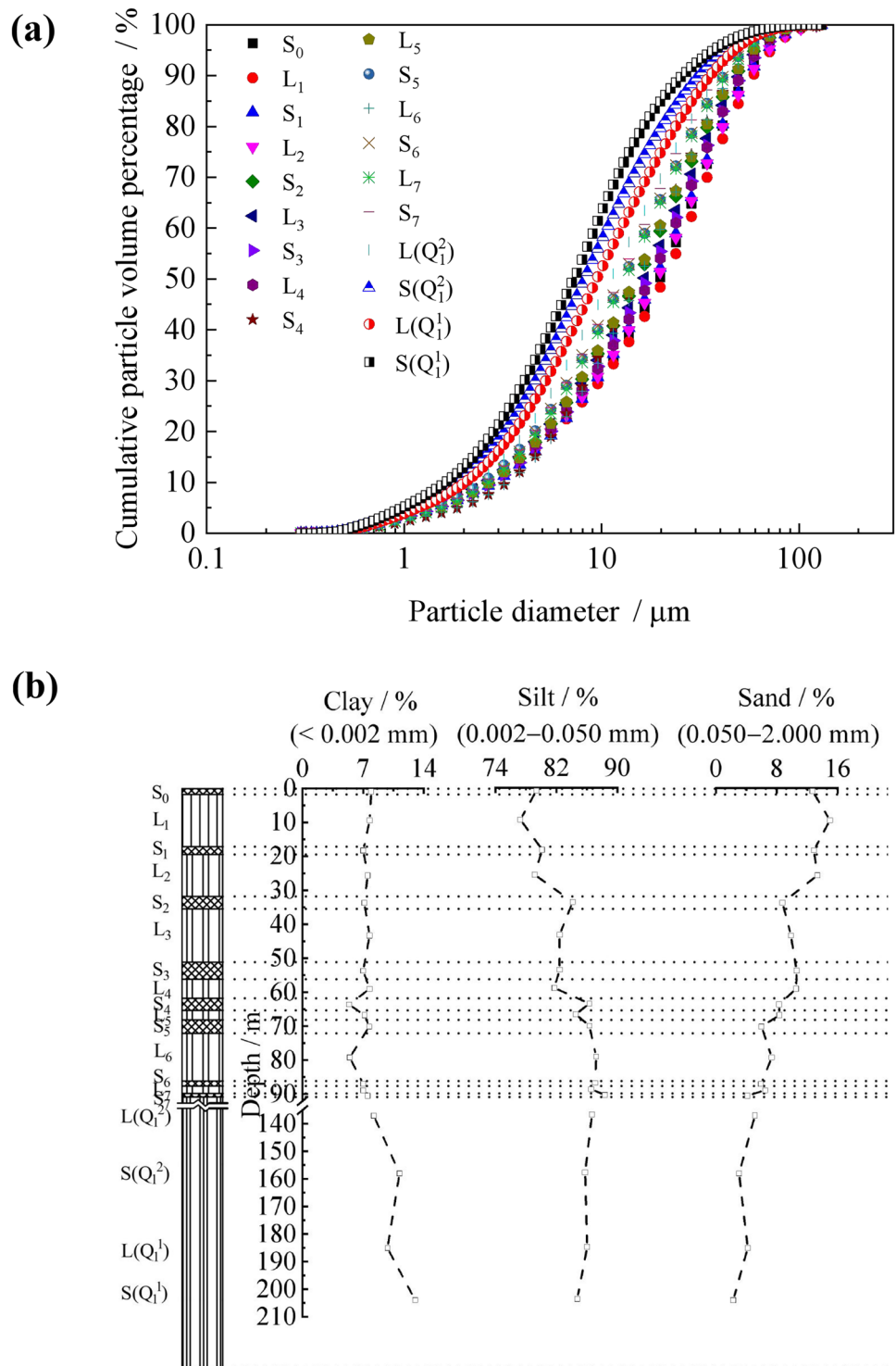
while the sand content tended to decrease. Furthermore, compared with the underlying loess, the sand content of the paleosol was smaller, while the clay content had not significantly different. From Q_4 to Q_2 strata, the silt content of the paleosol was greater than that of the underlying loess. However, the silt content of the paleosol in the Q_1 strata was slightly less than that of the underlying loess, due to higher clay content in the paleosol in the Q_1 strata than that of the underlying loess.

The dry density of loess ranged from 1.42 to 1.73 g/cm³, and that of paleosol ranged from 1.44 to 1.82 g/cm³ (Fig. 8). From Q_4 to Q_1 strata, the dry density of loess and paleosol had an overall increasing trend. The dry density fluctuated regularly with increasing depth. The peak was in the paleosol, and the trough was in the underlying loess, indicating higher dry density of the paleosol than that of the underlying loess. However, there was a negative correlation between the void ratio and dry density. The void ratio of loess varied in 0.57–0.90, and that of paleosol ranged from 0.51 to 0.88. The void ratio of loess and paleosol decreased significantly from top to bottom, and the void ratio also followed the fluctuation patterns. The trough appeared in the paleosol, and the peak appeared in the underlying loess, which proved that the void ratio of the paleosol was smaller than that of the underlying loess.

The water content of loess ranged from 16.3 to 20.8%, and that of paleosol ranged from 14.8 to 22.9%. The saturation range of loess was 45.5–84.6%, and that of paleosol was 60.2–93.2%. When the buried depth was greater than 62 m, the saturation of loess and paleosol was about 80%. It could be judged that the groundwater level is about 62 m deep, which can be regarded as the depth of saturation affected by the external environment. Moreover, from Q_4 to Q_1 strata, the saturation of loess and paleosol showed an increasing trend. The saturation fluctuated regularly with increasing depth, and the saturation of most paleosols was greater than that of the underlying loess. However, the fluctuation law of water content from Q_4 to Q_1 strata was bounded by the groundwater level, which was different from that of saturation. In the strata above the groundwater level, the peak appeared in the paleosol and the trough appeared in the underlying loess, indicating higher water content of the paleosol than that of the underlying loess. But in the strata below the groundwater level, the trough was in the paleosol and the peak was in the underlying loess, indicating lower water content of the paleosol than that of the underlying loess.

The specific gravity of loess ranged from 2.70 to 2.72, and that of paleosol ranged from 2.71 to 2.74, all showing a slight increase with depth. Moreover, the liquid limit of loess and paleosol all increased with increasing depth. The liquid limit of loess was 27.3–33.5%, and the plastic

Fig. 7 Particle sizes of loess-paleosol sequence in Zaosheng profile. **a** Particle grading curves. **b** Longitudinal distribution of particle sizes



limit was 17.1–19.4%. The liquid limit of paleosol was 30.3–44.5%, and the plastic limit was 18.6–21.4%. The peaks and troughs of the liquid plastic limit appeared alternately with increasing depth, and the liquid plastic limit of the paleosol was greater than that of the underlying loess.

Mechanical properties of loess-paleosol sequence

From Q_4 to Q_1 strata, the self-weight collapsibility coefficient showed regular fluctuation patterns with increasing depth (Fig. 9). The trough was in the paleosol, and the peak was in the underlying loess. The self-weight collapsibility

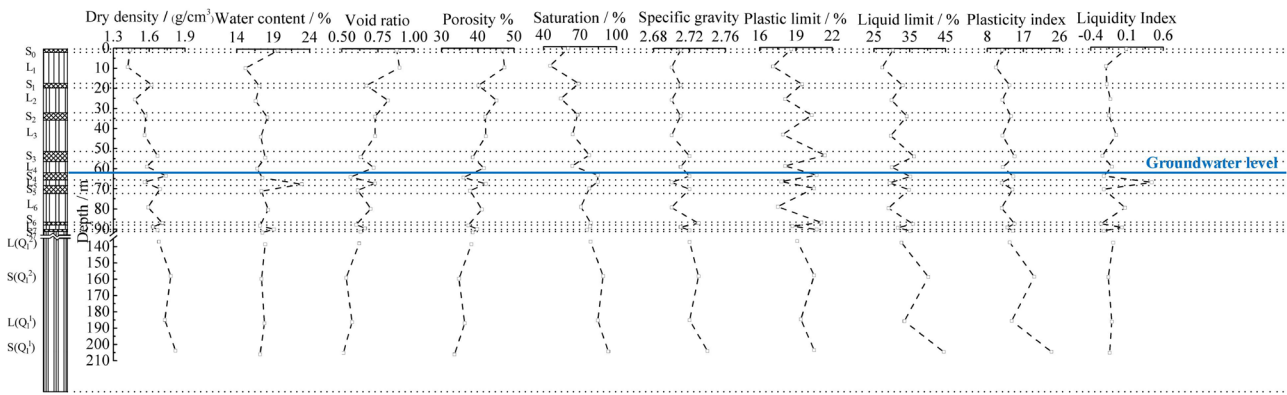


Fig. 8 Physical property indexes of loess-paleosol sequence in Zaosheng profile

coefficients of the paleosol from the Q₄ strata and the loess from the Q₃ strata and the L₂ layer of the Q₂ strata were all greater than 0.015 (0.017–0.029). Based on the China National Standards GB/T 50123–2019 (SAC 2019), these soils were considered collapsible soils. Furthermore, the self-weight collapsibility coefficient of the loess in the middle and lower parts of the Q₂ strata and the Q₁ strata was 0.001–0.012, and the self-weight collapsibility coefficient of the paleosol from Q₃ to Q₁ strata was 0, and their values were all less than 0.015. These soils were considered non-collapsible soils. Therefore, only the paleosol in the Q₄ strata and the loess in the Q₃ strata and the top of the Q₂ strata were collapsible.

The range of the free swelling ratio in loess was 19–23%, and that in paleosol was 29–64%. From Q₄ to Q₁ strata, the free swelling ratio fluctuated regularly with increasing depth. The peak was in the paleosol, and the trough was in the underlying loess. The free swelling ratio of the paleosol in the S₀ layer and the loess from Q₄ to Q₁ strata was less than 40%, so they were not swelling soils, while the free swelling ratio of other paleosols ranged from 40 to 65%. According to the China National Standards GB 50112–2013

(SAC 2013), these paleosols were swelling soils with weak swelling potential. Therefore, in engineering construction, attention should be paid not only to the collapsibility of the paleosol in the Q₄ strata and the loess in the Q₃ strata and the top of the Q₂ strata, but also to the swelling of the paleosol from Q₃ to Q₁ strata.

The cohesion of loess varied from 19.0 to 46.9 kPa, and that of paleosol varied from 19.6 to 66.3 kPa. The internal friction angle of loess ranged from 23.2° to 27.9°, and that of paleosol ranged from 20.9° to 31.5°. From Q₄ to Q₁ strata, the cohesion of loess and paleosol had an overall tendency to increase. The cohesion fluctuated regularly with increasing depth, and the cohesion of the paleosol was significantly greater than that of the underlying loess. However, the fluctuation of the internal friction angle with increasing depth was opposite to that of the cohesion. From Q₄ to Q₁ strata, the internal friction angle of loess and paleosol only increased slightly. The internal friction angle fluctuated slightly with increasing depth, and the internal friction angle of the paleosol was smaller than that of the underlying loess.

The compressibility of loess ranged from 0.110 to 0.197 MPa⁻¹, and that of paleosol ranged from 0.070 to

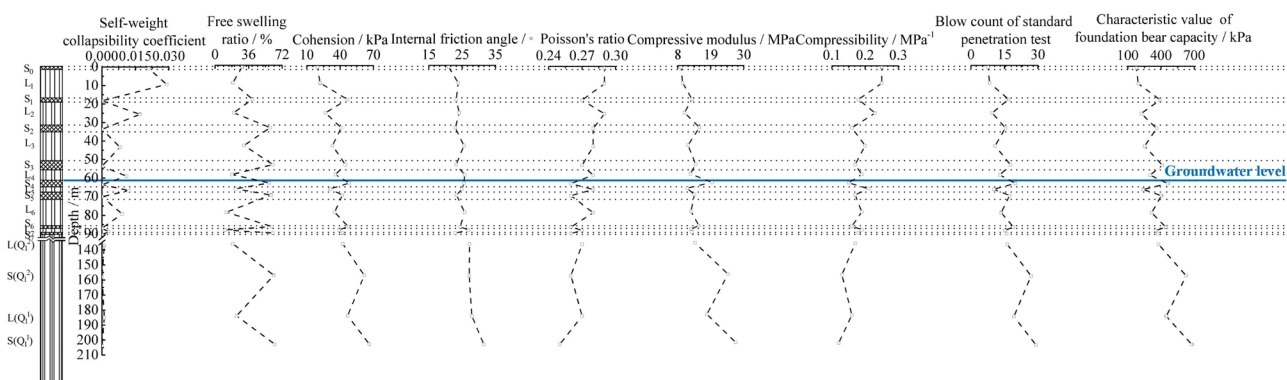


Fig. 9 Mechanical properties of loess-paleosol sequence in Zaosheng profile

0.204 MPa⁻¹. The compressive modulus of loess ranged from 9.55 to 17.70 MPa, and that of paleosol ranged from 9.12 to 27.30 MPa. From Q₄ to Q₁ strata, the compressibility of loess and paleosol tended to decrease as a whole, and the compressibility fluctuated regularly with increasing depth. The trough was in the paleosol, and the peak was in the underlying loess, indicating smaller compressibility of the paleosol than that of the underlying loess. However, the variation pattern of compressive modulus was opposite to that of compressibility. In addition, in the standard penetration test, the blow counts of loess ranged from 8.3 to 19.2, and those of paleosol ranged from 7.6 to 29.1. The characteristic value of foundation bearing capacity of loess varied from 193.39 to 447.36 kPa, and that of paleosol varied from 177.08 to 678.03 kPa. From Q₄ to Q₁ strata, the characteristic value of foundation bearing capacity in loess and paleosol had an overall increasing trend. The characteristic value of foundation bearing capacity fluctuated regularly with increasing depth. The peak was in the paleosol and the trough was in the underlying loess, indicating that the characteristic value of foundation bearing capacity of the paleosol was larger than that of the underlying loess.

When the embedded depth of the foundation is greater than 0.5 m, the characteristic value of foundation bearing capacity determined from the standard penetration test should be corrected by the following equation (Chang and Zhang 2018):

$$f_a = f_{ak} + \eta_b \gamma (b - 3) + \eta_d \gamma_m (d - 0.5) \quad (1)$$

where f_a is the modified characteristic value of foundation bearing capacity, kPa; f_{ak} is the characteristic value of foundation bearing capacity, kPa; η_b and η_d are the correction coefficients; γ is the unit weight of the soil below the foundation bottom, kN/m³, and the unit weight of the soil below the groundwater level is the effective unit weight; b is the width of the foundation bottom, m , and b is 3 m when the width of the foundation bottom is less than 3 m and b is 6 m when the width of the foundation bottom is greater than 6 m; γ_m is the average unit weight of the soil above the foundation bottom, kN/m³, and the unit weight of the soil below the groundwater level is the effective unit weight; and d is the embedded depth of the foundation, m .

Based on Eq. (1), it could be judged that under the same foundation, the relationship between the loess and adjacent paleosol in the modified characteristic value of foundation bearing capacity is consistent with that in the characteristic value of foundation bearing capacity. The influence of the groundwater level on the modified characteristic value of foundation bearing capacity was analyzed under the assumption that the foundation buried deeper than 0.5 m is equal in each layer. In the Q₂ strata, although the dry density of the paleosol below the groundwater level tended to increase,

due to the increase in saturation and water content, the characteristic value of foundation bearing capacity of the paleosol below the groundwater level was not significantly different from but even smaller than that of the paleosol above and near the groundwater level (Fig. 9). When modifying the characteristic value of foundation bearing capacity based on Eq. (1), the $\eta_b \gamma (b-3)$ and $\eta_d \gamma_m (d-0.5)$ of the paleosol below the groundwater level are significantly smaller than the $\eta_b \gamma (b-3)$ and $\eta_d \gamma_m (d-0.5)$ of the paleosol above and nearby the groundwater level, respectively. Thus, it could be inferred that in the Q₂ strata, the modified characteristic value of foundation bearing capacity of the paleosol below the groundwater level is smaller than that of the paleosol above and nearby the groundwater level. Similarly, the modified characteristic value of foundation bearing capacity of the Q₂ loess below the groundwater level also should be smaller than that of the loess above and nearby the groundwater level. In addition, the paleosol in the Q₁ strata was below the groundwater level, and the characteristic value of foundation bearing capacity of the paleosol in the Q₁ strata was much larger than that of the paleosol above and nearby the groundwater level due to the increase in dry density (Fig. 9). When modifying the characteristic value of foundation bearing capacity based on Eq. (1), the $\eta_b \gamma (b-3)$ and $\eta_d \gamma_m (d-0.5)$ of the paleosol in the Q₁ strata are obviously smaller than the $\eta_b \gamma (b-3)$ and $\eta_d \gamma_m (d-0.5)$ of the paleosol above and nearby the groundwater level, respectively. Therefore, it could be inferred that the modified characteristic value of foundation bearing capacity of the paleosol in the Q₁ strata is not much larger but even smaller than that of the paleosol above and nearby the groundwater level. The same conclusion can also be applied to the relationship between the modified characteristic value of foundation bearing capacity of the loess in the Q₁ strata and that of the loess above and nearby the groundwater level.

Discussions

Relationship between physical and chemical properties

Based on the chemical properties, the reasons for the distribution of physical properties of the loess-paleosol sequence in the Zaosheng profile were discussed. It can be seen from Fig. 10 that the major element compositions in the Zaosheng profile only vary slightly. The major elements were SiO₂, Al₂O₃, CaO, and Fe₂O₃, and the sum of the four elements was greater than 75%. Thus, the element compositions of the loess-paleosol sequence in the Zaosheng profile were similar to those in the Jiuzhoutai profile and Luochuan profile (Bronger and Heinkele 1989; McIntosh et al. 1996; Sun 2005), indicating that the loess and paleosol in the Zaosheng

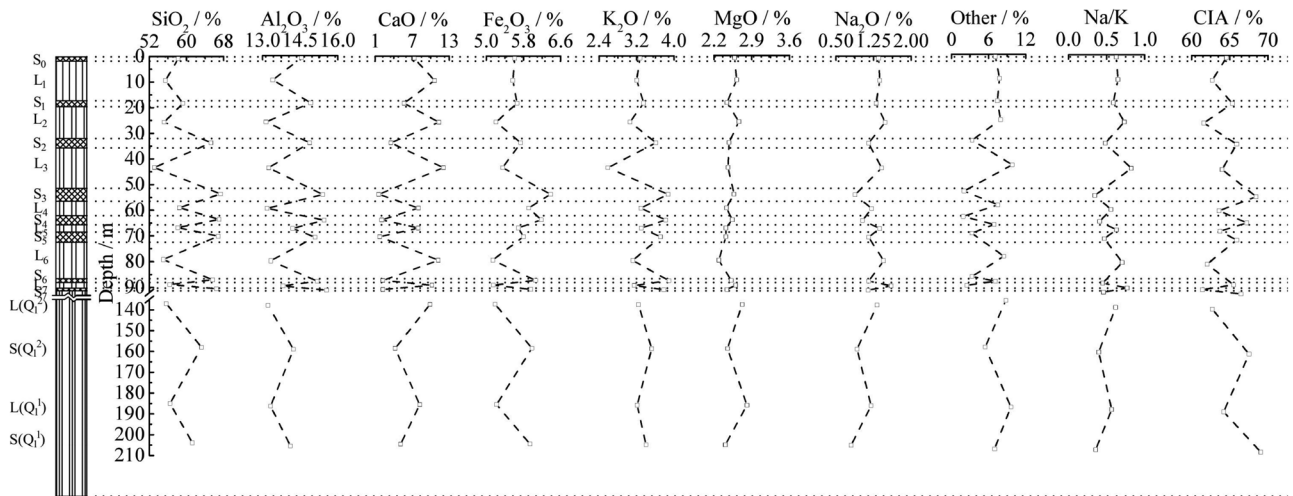


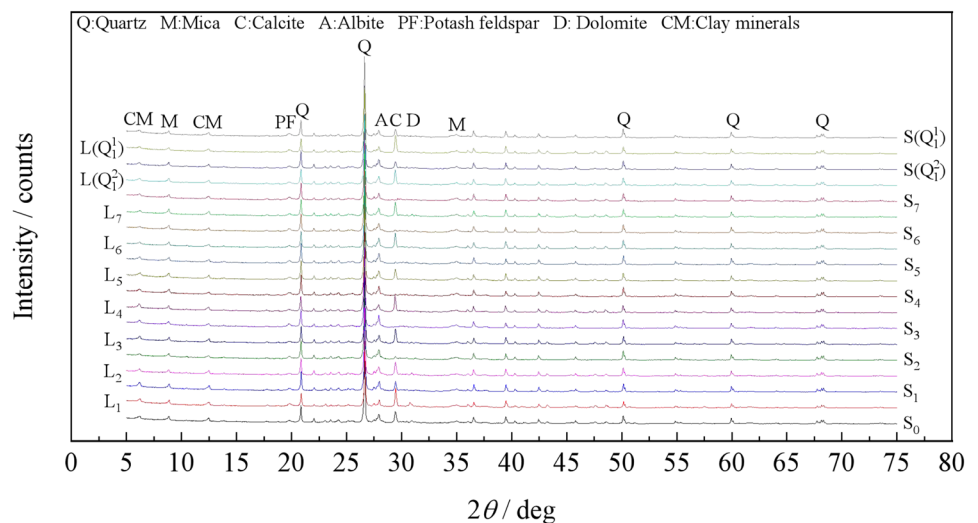
Fig. 10 Element compositions of loess-paleosol sequence in Zaosheng profile

tableland are of aeolian origin. Moreover, the Chemical Index of Alteration (CIA) and Na/K ratio are commonly used indicators to judge the weathering degree (Nesbitt and Young 1982; Guo et al. 2018). The calculation formula of CIA is $[Al_2O_3 / (Al_2O_3 + CaO^* + K_2O + Na_2O)] \times 100$, where each oxide is in the unit of its mole number. In general, the CIA value of 50–65 indicates a weak degree of chemical weathering, and the climatic conditions for forming the soil are cold and dry. And the CIA value of 65–85 implies an intermediate chemical weathering of soil, which requires warm and humid climate conditions. It could be judged that the loess in the Zaosheng profile is in the degree of weak chemical weathering, while the paleosol is in the degree of intermediate chemical weathering.

Feldspar minerals have high hardness and light color, which keeps them away from being affected by physical

weathering but makes them prone to chemical weathering (Wild et al. 2016), which belong to unstable minerals. Calcite is a mineral with low hardness and is susceptible to chemical and physical weathering (Villagran and Poch 2014). The formation of the paleosol required a warm and humid climate, and adequate precipitation. In this stage, the chemical weathering of potash feldspar, albite, and calcite was very likely to occur, which might lead to decreasing content, while the products of this stage were clay minerals (Brindley 1981; Garcia et al. 2012), which would have accumulated. These patterns also applied to the variations of Figs. 11 and 12. For potash feldspar, albite, and calcite, their contents were found to fluctuate regularly with increasing depth, with troughs in the paleosol and the peaks in the underlying loess. For clay minerals, regular fluctuations with increasing depth were also observed, while the peaks were

Fig. 11 X-ray diffraction patterns of loess-paleosol sequence in Zaosheng profile



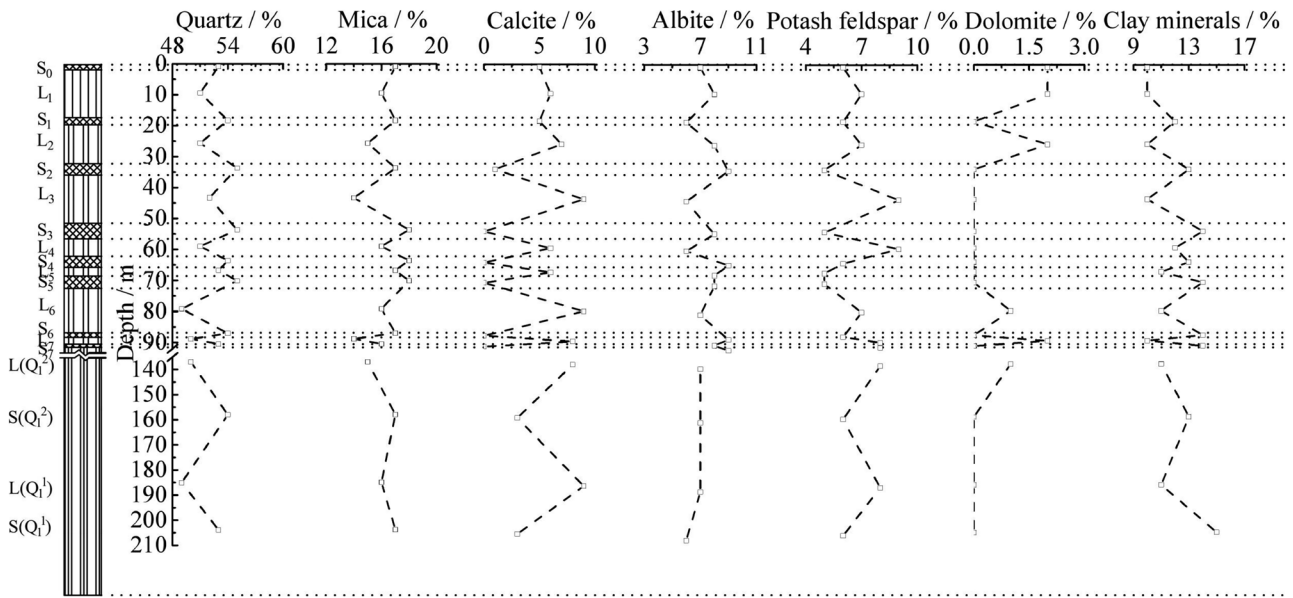


Fig. 12 Mineral compositions of loess-paleosol sequence in Zaosheng profile

found in the paleosol and the troughs were identified in the underlying loess. In loess and paleosol, albite and calcite are coarse-grained minerals, while clay minerals are fine-grained minerals (Brindley 1981; Garcia et al. 2012). Hence, compared with the particle size in the underlying loess, the paleosol experienced intermediate chemical weathering with relatively fewer coarse particles (sand) and more fine particles (clay and silt) (Fig. 7).

The large specific surface area of fine particles (Hepper et al. 2006; Zhu et al. 2022) equips them with strong adsorption capacity, and the inlaid filling of large pores by fine particles blocks the water flow channel in the soil. Therefore, the increase in fine particles is usually accompanied by slower water flow velocity in the soil and higher water storage capacity, which would lead to greater specific gravity and liquid plastic limit. In addition, when the fine particle content is high, the coarse particles tend to be evenly distributed in the fine particle matrix, the soil particles are filled with fine particles, and the coarse particles are separated. This is conducive to the directional arrangement of particles and the increase in pellicular water content, thus increasing the specific gravity and liquid plastic limit of the soil (Dolinar and Trauner 2004). That is, the specific gravity and liquid plastic limit of soil are significantly positively correlated with the fine particle content. Hence, due to the greater fine particle content of the paleosol than that of the underlying loess, and the simultaneous increase in the fine particle content of both loess and paleosol with increasing depth (Fig. 7), the specific gravity and liquid plastic limit of the paleosol were larger than those of the underlying loess, and the specific gravity and liquid plastic limit of loess and

paleosol had an increasing trend with the increase in depth (Fig. 8).

Distribution of chemical and physical properties in the Loess Plateau

The comparative analysis of CIA and Na/K of loess and paleosol in the Loess Plateau is shown in Fig. 13 (Zhang et al. 1991; Diao and Wen 1999; Chen et al. 2001, 2008). The chemical weathering intensity of Zhenjiang loess is the highest, followed by Weinan paleosol, and that of Lanzhou loess is the lowest. From the northwest to the southeast of the Loess Plateau (Fig. 1), the chemical weathering intensity of loess and paleosol tends to

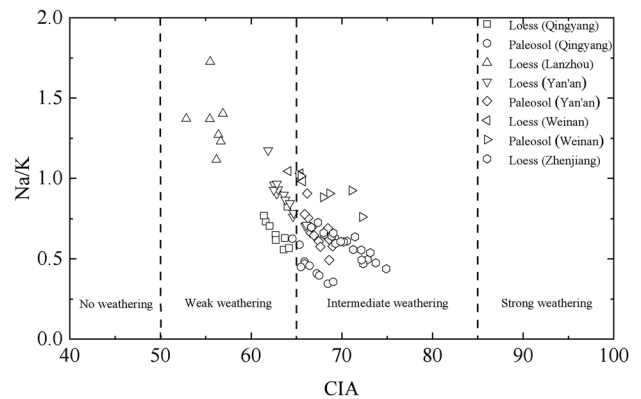


Fig. 13 Chemical weathering intensities of loess-paleosol sequence in the Loess Plateau

increase, and the chemical weathering intensity of paleosol in the same place is greater than that of loess. Thus, from the northwest to the southeast of the Loess Plateau, the contents of potash feldspar, albite, and calcite in loess and paleosol have a decreasing trend, while the contents of clay minerals have an increasing trend. It could be inferred that from the northwest to the southeast of the Loess Plateau, the clay content of loess and paleosol tends to increase, while the sand content tends to decrease. Previous studies have demonstrated that Q₃ loess has a consistent trend (Sun 2005). Samples were taken from Q₄ to Q₁ strata of the Jiuzhoutai profile in Lanzhou, and their particle sizes were tested and compared with those of samples in Qingyang, Yan'an (Ding et al. 2000), and Xi'an (Liang et al. 2016). It could be found that from the northwest to the southeast of the Loess Plateau, the clay content of loess and paleosol in Q₄ to Q₁ strata has an increasing trend, and the sand content has a decreasing trend (Figs. 1 and 14).

Samples were taken from Q₄ to Q₁ strata of the Jiuzhoutai profile in Lanzhou, and their liquid plastic limits were tested and compared with those of samples in Qingyang, Yan'an (Wang et al. 2015), Xianyang (Tu et al. 2010), and Baoji (Tan et al. 2015) (Fig. 15). From the northwest to the southeast of the Loess Plateau, the clay content of the paleosol and loess in Q₄ to Q₁ strata has a consistently increasing trend, so the liquid limit and plasticity index tend to increase, which are the same as the variations in Fig. 15.

In Lanzhou, Yan'an, Xi'an, Xianyang, and Baoji of the Loess Plateau, a small amount of data showed that the variations of loess and paleosol with increasing depth in terms of particle size and plasticity properties were not in

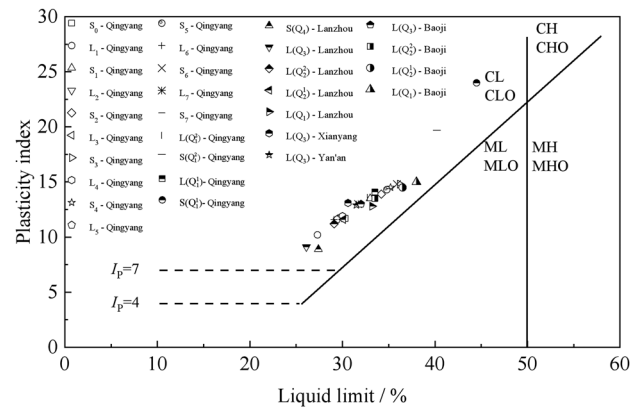
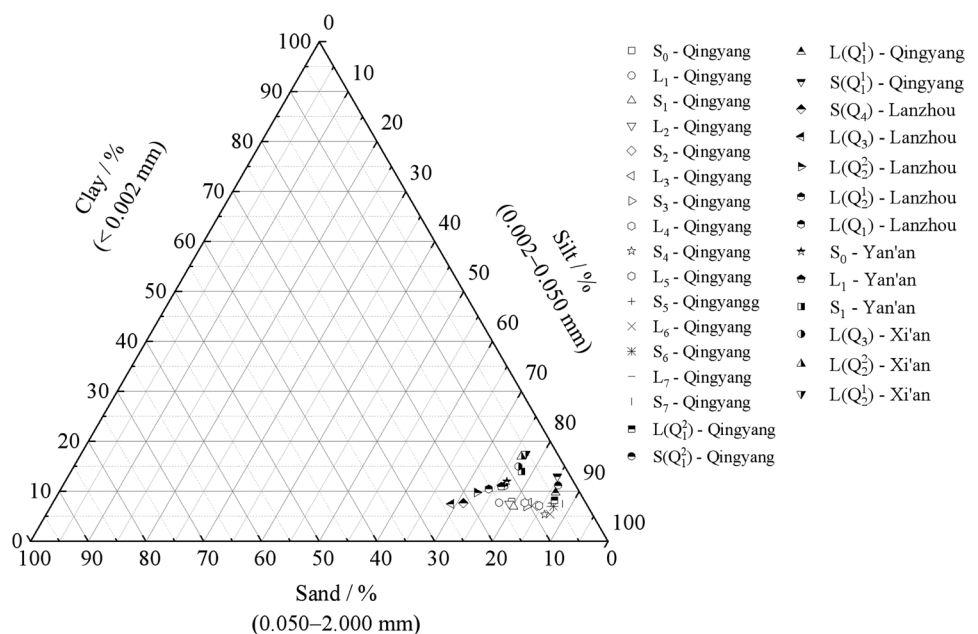


Fig. 15 Plasticity properties of loess-paleosol sequence in the Loess Plateau

contradiction with the laws obtained in this study (Figs. 14 and 15). It could be speculated that the distribution of particle size and plasticity properties of the loess-paleosol sequence in the Zaosheng profile can represent that in deep loess strata in many places of the Loess Plateau. Moreover, particle size and plasticity properties are the most basic physical properties, which can affect many related physico-mechanical properties (Zhang et al. 2018; Liu et al. 2022; Zhu et al. 2022). The distribution and thickness of the loess-paleosol sequence in the Zaosheng profile conform to the strata distribution characteristics of the whole Loess Plateau (Fig. 6). Thereby, it was reasonable to believe that the longitudinal distribution of the physico-mechanical properties of the deep loess strata in many places of the Loess Plateau should be consistent with that of the Zaosheng profile.

Fig. 14 Particle sizes of loess-paleosol sequence in the Loess Plateau



Relationship between physical properties and microstructures

During the loess accumulation period, the climate was cold and dry, and the loess had weak pedogenesis, few fine particles, many macropores, and a loose structure (Fig. 16). However, during the paleosol formation, the climate was warm and humid, and the paleosol had strong pedogenesis. Affected by rainwater leaching (Sylvain et al. 1996; Björn et al. 2011; Huang et al. 2018), the soluble salts and unstable minerals in the paleosol were leached away, and the fine-grained materials formed by the secondary effect filled the macropores, making the structure denser than that of the underlying loess, resulting in smaller porosity and larger dry density. That is, the dry density of the paleosol was greater than that of the underlying loess (Fig. 8). Moreover, the variation of density, dry density, and void ratio with increasing depth was largely due to the continuous accumulation of loess and paleosol. With the increase in overburden pressure, the loess and paleosol particles were more closely arranged, indicating the compaction effect of the consolidation pressure.

In the strata above the groundwater level, the relatively large pores of loess promoted water to migrate downward and be stored in the paleosol with relatively small pores (Fig. 16). Loess had few fine particles and clay minerals

with large specific surface area and was not easy to absorb water (Hepper et al. 2006; Zhu et al. 2022). As a result, the underlying loess was permeable, the paleosol was weakly permeable, and the water content of the underlying loess was smaller than that of the paleosol (Fig. 8). However, in the strata below the groundwater level, the loess and paleosol were saturated. The pores of the underlying loess were larger and more than those of the paleosol; thus, the underlying loess was easier to store water than the paleosol, and the water content of the underlying loess was greater than that of the paleosol. In addition, compared with the underlying loess, the paleosol contained more fine particles and clay minerals with large specific surface area, and had a stronger ability to absorb water per unit area (Hepper et al. 2006; Zhu et al. 2022), which resulted in greater pore water storage per unit area in the paleosol. Therefore, from Q₄ to Q₁ strata, the saturation of the paleosol was greater than that of the underlying loess.

Relationship between mechanical properties and microstructures

Through quantitative analysis of Fig. 16, the number of pores, apparent porosity, and fractal dimension were obtained (Table 1). During the compression and standard penetration tests, the variation of the soil volume is

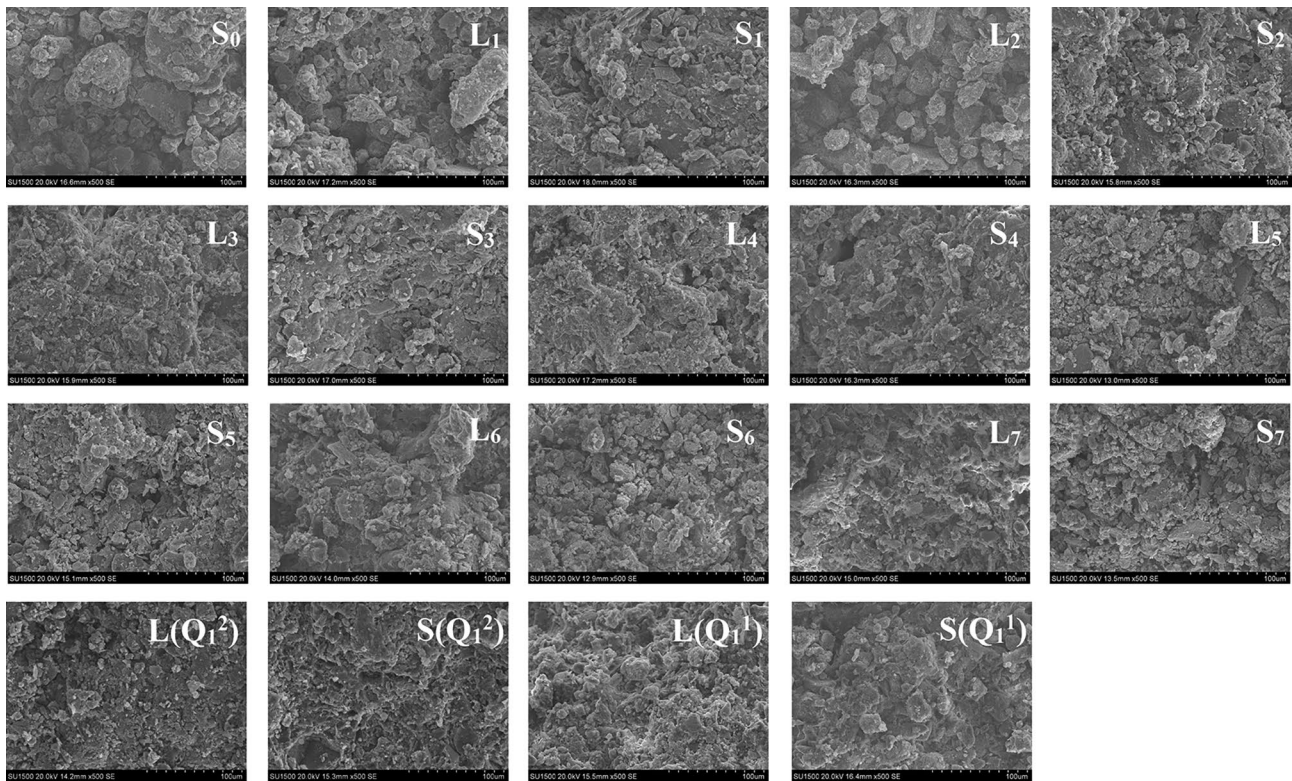


Fig. 16 Microstructures of loess-paleosol sequence in Zaosheng profile

Table 1 Quantitative analysis of microstructure for loess-paleosol sequence in Zaosheng profile

| Layer | Number of pores | Apparent porosity / % | Fractal dimension |
|---------------------------------|-----------------|-----------------------|-------------------------|
| S ₀ | 632 | 16.7 | 1.1411 ($R^2=0.9947$) |
| L ₁ | 658 | 16.7 | 1.1458 ($R^2=0.9938$) |
| S ₁ | 594 | 7.3 | 1.0834 ($R^2=0.9977$) |
| L ₂ | 638 | 15.3 | 1.1168 ($R^2=0.9958$) |
| S ₂ | 627 | 8.1 | 1.0848 ($R^2=0.9978$) |
| L ₃ | 605 | 10.6 | 1.1104 ($R^2=0.9966$) |
| S ₃ | 599 | 6.8 | 1.0821 ($R^2=0.9979$) |
| L ₄ | 582 | 9.9 | 1.0872 ($R^2=0.9972$) |
| S ₄ | 522 | 6.1 | 1.0691 ($R^2=0.9982$) |
| L ₅ | 598 | 11.4 | 1.1010 ($R^2=0.9968$) |
| S ₅ | 617 | 7.0 | 1.0861 ($R^2=0.9976$) |
| L ₆ | 609 | 9.8 | 1.0956 ($R^2=0.9971$) |
| S ₆ | 580 | 6.8 | 1.0725 ($R^2=0.9975$) |
| L ₇ | 586 | 8.0 | 1.0797 ($R^2=0.9972$) |
| S ₇ | 615 | 7.5 | 1.0840 ($R^2=0.9980$) |
| L(Q ₁ ²) | 558 | 7.1 | 1.0743 ($R^2=0.9945$) |
| S(Q ₁ ²) | 495 | 5.7 | 1.0633 ($R^2=0.9965$) |
| L(Q ₁ ¹) | 529 | 6.0 | 1.0651 ($R^2=0.9984$) |
| S(Q ₁ ¹) | 472 | 5.2 | 1.0611 ($R^2=0.9979$) |

mainly due to the pore compression in the soil. It can be seen from Table 1 that from Q₄ to Q₁ strata, the number of pores in loess decreases from 658 to 529, and that in paleosol decreases from 632 to 472; the apparent porosity of loess decreases from 16.7 to 6.0%, and that of paleosol decreases from 16.7 to 5.2%. From Q₄ to Q₁ strata, the content of inter-particle pores decreased in general, especially the trellis pores decreased or even disappeared, and the particles in the soil were arranged more closely, so the anti-compression capacity and characteristic value of foundation bearing capacity of loess and paleosol increased (Fig. 9). Compared with the underlying loess, the pore content of the paleosol was smaller and the particle arrangement was more compact, resulting in greater anti-compression capacity and characteristic value of foundation bearing capacity of the paleosol.

As can be seen from Fig. 16 and Table 1, from Q₄ to Q₁ strata, the contact mode between particles develops from point-to-point contact, point-to-surface contact to surface-to-surface contact, and the cementation between particles becomes more obvious, which increases the cohesion of loess and paleosol (Fig. 9). Compared with the underlying loess, the cementation between the particles in the paleosol was stronger, causing stronger cohesion of the paleosol. In addition, the fractal dimension of the paleosol was smaller than that of the underlying loess, indicating that the edges and angles of the mineral debris in the paleosol became less obvious than those in the underlying loess. Thus, the

internal friction angle between the paleosol particles was smaller than that between the underlying loess particles. On the one hand, from Q₄ to Q₁ strata, the fractal dimension of loess decreased from 1.1458 to 1.0651, that of paleosol decreased from 1.1411 to 1.0611, and the edges and angles of mineral debris became less obvious. On the other hand, from Q₄ to Q₁ strata, the arrangement of loess and paleosol particles was closer, and the pore content between particles was generally reduced. The role of this aspect on the internal friction angle was slightly greater than that of the previous aspect. Thus, on the whole, the internal friction angle of loess and paleosol displayed no obvious variation from Q₄ to Q₁ strata, but only slightly increased.

The paleosol in the Q₄ strata and the loess in the Q₃ strata and the top of the Q₂ strata had large and many trellis pores, and the degree of cementation between the particles was weak. When they encountered water, the cementation between the particles was destroyed. The particles migrated relatively, small particles entered the trellis pores, and the soil structure was destroyed, causing the whole soil to collapse (Karl 2001; Zhuang et al. 2018), while the paleosol from Q₃ to Q₁ strata and the loess in the middle and lower parts of the Q₂ strata and the Q₁ strata had small or no trellis pores. The degree of cementation between the particles was strong, and its structure was not easily damaged when encountering water, which could prevent the whole soil from collapsing obviously. Therefore, only the paleosol in the Q₄ strata and the loess in the Q₃ strata and the top of the Q₂ strata were collapsible (Fig. 9). In addition, the paleosol from Q₃ to Q₁ strata had dense structure, strong pedogenesis, and high clay mineral content. When the paleosol from Q₃ to Q₁ strata encountered water, the structure was not likely to collapse, and clay minerals were prone to swell (Brindley 1981; Garcia et al. 2012), resulting in the swelling of the whole soil. In other words, the paleosol from Q₃ to Q₁ strata belonged to swelling soil.

Conclusions

This study determined the longitudinal distribution of physico-mechanical properties of the loess-paleosol sequence from Q₄ to Q₁ strata in the Zaosheng profile. Based on the relationship between chemical properties, microstructures, and physico-mechanical properties, the underlying mechanisms for the variations in physico-mechanical properties of the loess-paleosol sequence were discussed. Meanwhile, the distribution of chemical and physical properties of the loess-paleosol sequence in the Loess Plateau was determined. Based on this study, the main conclusions are presented as follows.

1. From Q_4 to Q_1 strata, the dry density, saturation, specific gravity, and liquid limit of loess and paleosol had an overall increasing trend, and these parameters of the paleosol were greater than those of the underlying loess. However, the fluctuations of water content with depth were inconsistent with those of these parameters. In the strata above the groundwater level, the water content of the paleosol was greater than that of the underlying loess. But in the strata below the groundwater level, the water content of the paleosol was less than that of the underlying loess.
2. From Q_4 to Q_1 strata, the compressive modulus, characteristic value of foundation bearing capacity, and cohesion of loess and paleosol had an overall increasing trend. These parameters of the paleosol were greater than those of the underlying loess. However, from Q_4 to Q_1 strata, the internal friction angle of loess and paleosol only increased slightly, and the internal friction angle of the paleosol was less than that of the underlying loess. Moreover, the paleosol in the Q_4 strata and the loess in the Q_3 strata and the top of the Q_2 strata were collapsible soils, and the paleosol in Q_3 to Q_1 strata was swelling soil.
3. From Q_4 to Q_1 strata, the content of inter-particle pores in loess and paleosol gradually decreased, and the particle arrangement gradually became tighter, but the edges and angles of the particle debris became less obvious. Compared with the underlying loess, the paleosol had better cementation between particles and smaller pore content, but the edges and angles of the particle debris were less obvious. The microstructure of loess and paleosol corresponded exactly to the macroscopic mechanical properties.
4. The chemical weathering intensity of paleosol (intermediate) was stronger than that of loess (weak). The potash feldspar, albite, and calcite of the paleosol were smaller than those of the underlying loess, but the clay minerals of the paleosol were larger than those of the underlying loess. These could explain the longitudinal distribution of physical properties (particle size, specific gravity, liquid plastic limit, and saturation) of the loess-paleosol sequence along with the depth.
5. The increase in chemical weathering intensity from northwest to southeast Loess Plateau would, therefore, contribute to lower (higher) clay content, liquid limit, and plastic index of the loess and paleosol in Q_4 to Q_1 strata in the northwest (southeast), and decreasing sand content in the corresponding direction.

Funding All authors are grateful for the financial support provided by the Fundamental Research Funds for the Central Universities of China (No. lzujbky-2017-ct02, lzujbky-2018-it24), and Science and Technology Research and Development Program of China Railway Corporation (No. 2017G007-G).

Declarations

Conflict of interest The authors declare no competing interests.

References

- Björn B, Bruno G, Ulrich H, Natali G, Slobodan M (2011) An evaluation of geochemical weathering indices in loess-paleosol studies. *Quat Int* 240:12–21
- Brindley GW (1981) *Clays, clay minerals*. Springer, US, New York
- Bronger A, Heinkele T (1989) Micromorphology and genesis of paleosols in the Luochuan loess section, China: Pedostratigraphic and environmental implications. *Geoderma* 45(2):123–143
- Chang SB, Zhang SM (2018) *Geological engineering handbook*. China Architecture & Building Press, Beijing (in Chinese)
- Chen J, An ZS, Head J (1999) Variation of Rb/Sr ratios in the loess-paleosol sequences of central China during the last 130,000 years and their implications for monsoon paleoclimatology. *Quat Res* 51(3):215–219
- Chen J, An ZS, Liu LW, Ji JF, Yang JD, Chen Y (2001) Variations in chemical compositions of the eolian dust in chinese loess plateau over the past 2.5 ma and chemical weathering in the asian inland. *Sci China Ser D* 05:21–31
- Chen YY, Li XS, Han ZY, Yang SY, Wang YB, Yang DY (2008) Chemical weathering intensity and element migration features of the xiashu loess profile in zhenjiang, jiangsu province. *J Geogr Sci* 18(3):341–352
- Diao G, Wen QZ (1999) Mobility sequence of chemical elements during loess weathering-pedogenesis, Weinan, Shaanxi Province, China. *Chin J Geochem* 18(4):327–332
- Ding ZL, Rutter NW, Sun JM, Yang SL, Liu TS (2000) Re-arrangement of atmospheric circulation at about 2.6 ma over northern china: evidence from grain size records of loess-paleosol and red clay sequences. *Quat Sci Rev* 19(6):547–558
- Dolinar B, Trauner L (2004) Liquid limit and specific surface of clay particles. *Geotech Test J* 27(6):580–584
- Fratta D, Alshibli KA, Tanner WM, Roussel L (2005) Combined TDR and P-wave velocity measurements for the determination of in situ soil density – experimental study. *Geotech Test J* 28(6):553–563
- Garcia GR, Villa RVDL, González MJA (2012) Characterization of loess in central Spain: a microstructural study. *Environ Earth Sci* 65:2125–2137
- Guo MM, Wang WL, Wang TC, Wang WX, Kang HL (2020) Impacts of different vegetation restoration options on gully head soil resistance and soil erosion in loess tablelands. *Earth Surf Process Landf* 45(4):1038–1050
- Guo YL, Yang SY, Su N, Li C, Yin P, Wang ZB (2018) Revisiting the effects of hydrodynamic sorting and sedimentary recycling on chemical weathering indices. *Geochim Cosmochim Acta* 227:48–63
- Hepper EN, Buschiazzi DE, Hevia GG, Urioste A, Antóna L (2006) Clay mineralogy, cation exchange capacity and specific surface area of loess soils with different volcanic ash contents. *Geoderma* 135:216–223
- Huang CQ, Wang MN, Tan WF, Wang MK, Koopal LK (2018) Hydroxy-interlayered minerals in the Holocene paleosol on the southernmost Loess Plateau, China. *Appl Clay Sci* 153:70–77
- Jahn B, Gallet S, Han JM (2001) Geochemistry of the Xining, Xifeng and Jixian sections, Loess Plateau of China: eolian dust provenance and paleosol evolution during the last 140 ka. *Chem Geol* 178(1–4):71–94
- Karl TR (2001) Late Holocene loess deposits and dust accumulation in the alpine meadow belt of the Wutai Shan. *China Quat Int* 76(77):85–92

- Leng YQ, Peng JB, Wang QY, Meng ZJ, Huang WL (2018) A fluidized landslide occurred in the Loess Plateau: A study on loess landslide in South Jingyang tableland. *Eng Geol* 236:129–136
- Li CB, Qi JG, Wang SB, Yang LS, Yang WJ, Zou SB, Zhu GF, Li WY (2014) A holistic system approach to understanding underground water dynamics in the loess tableland: a case study of the Dongzhi loess tableland in Northwest China. *Water Resour Manag* 28:2937–2951
- Li J, Wen XY, Huang CM (2020a) Lower and upper Cretaceous paleosols in the western Sichuan Basin, China: Implications for regional paleoclimate. *Geol J* 55:390–408
- Li L, Lan H, Peng J (2020b) Loess erosion patterns on a cut-slope revealed by lidar scanning. *Eng Geol* 268:105516
- Li XA, Wang L, Yan YL, Hong B, Li LC (2019) Experimental study on the disintegration of loess in the Loess Plateau of China. *Bull Eng Geol Environ* 78(7):4907–4918
- Liang QG, Li J, Wu XY, Zhou AN (2016) Anisotropy of Q₂ loess in the baijiapo tunnel on the lanyu railway, china. *Bull Eng Geol Environ* 75:109–124
- Liu TS (1985) *Loess and the environment*. Science Press, Beijing
- Liu W, Zhu J, Zhang H, Ma X, Xie J (2022) Geological conditions of saturated soft loess stratum and influence of tunnel excavation and dewatering system on its groundwater environment. *Bull Eng Geol Environ* 81:128
- Liu XM, Liu TS, Xu TC, Chen MY (1988) The Chinese loess in Xifeng, I. The primary study on magnetostratigraphy of a loess profile in Xifeng area, Gansu province. *Geophys J Int* 92(2):345–348
- McIntosh G, Rolph TC, Shaw J, Dagley P (1996) A detailed record of normal-reversed-polarity transition obtained from a thick loess sequence at Jiuzhoutai, near Lanzhou. *China Geophys J Int* 127(3):651–664
- Metelková Z, Boháč J, Přikryl R, Sedlářová I (2012) Maturation of loess treated with variable lime admixture: Pore space textural evolution and related phase changes. *Appl Clay Sci* 61:37–43
- Nesbitt HW, Young GM (1982) Early Proterozoic climates and plate motions inferred from major element chemistry of lutites. *Nature* 299:715–717
- Pei XJ, Zhang FY, Wu WJ, Liang SY (2015) Physicochemical and index properties of loess stabilized with lime and fly ash piles. *Appl Clay Sci* 114:77–84
- Standardization Administration of China (SAC) (2013) *China National Standards GB 50112–2013: Technical code for buildings in expansive soil regions*. China Planning Publishing House, Beijing (in Chinese)
- Standardization Administration of China (SAC) (2019) *China National Standards GB/T 50123–2019: Standard for soil test method*. China Planning Press, Beijing (in Chinese)
- Sun JZ (2005) *Loess science*. Hong Kong Archaeological Society Press, Hong Kong
- Sun P, Peng JB, Chen LW, Lu QZ, Igwe O (2016) An experimental study of the mechanical characteristics of fractured loess in western China. *Bull Eng Geol Environ* 75(4):1639–1647
- Sylvain G, Bor-ming J, Masayuki T (1996) Geochemical characterization of the Luochuan loess-paleosol sequence, China, and paleoclimatic implications. *Chem Geol* 133:67–88
- Tan CX, Sun WF, Meng J, Zhang CS, Wu SR, Shi JS, Li B, Wang T (2015) Research on loess-paleosol engineering geology features from the borehole cores of a typical section in Baoji area, Shaanxi province, China. *Environ Earth Sci* 74:4469–4491
- Tu XB, Dai FC, Akl K, Lg T, Xu L (2010) Causes of recurring landslides in loess plateau, Shaanxi Province, China. *Hkie Trans* 17(1):36–44
- Villagran XS, Poch RM (2014) A new form of needle-fiber calcite produced by physical weathering of shells. *Geoderma* 213:173–177
- Wang GL, Li TL, Xing XL, Zou Y (2015) Research on loess flow-slides induced by rainfall in July 2013 in Yan'an, Nw China. *Environ Earth Sci* 73:7933–7944
- Wang YY, Sadao S (1985) *The new development of loess studies in China*. Shaanxi people's publishing house, Xi'an (in Chinese)
- Wild B, Daval D, Guyot F, Knauss KG, Pollet-Villard M, Imfeld G (2016) pH-dependent control of feldspar dissolution rate by altered surface layers. *Chem Geol* 442:148–159
- Xi Y, Li TL, Jiang RJ, Lin XY (2018) Engineering geological stratigraphy and physical properties of the loess in eastern Gansu. *Hydrogeol Eng Geol* 45(4):67–72 (In Chinese)
- Xiong LY, Tang GA, Li FY, Yuan BY, Lu ZC (2014) Modeling the evolution of loess-covered landforms in the Loess Plateau of China using a DEM of underground bedrock surface. *Geomorphology* 209:18–26
- Xue XX, Zhang YX, Yue LP (2006) Paleoenvironments indicated by the fossil mammalian assemblages from red clay-loess sequence in the Chinese Loess Plateau since 8.0 Ma BP. *Sci China Ser D* 49(5):518–530
- Xue YG, Zhang XL, Li SC, Qiu DH (2019) Sensitivity analysis of loess stability to physico-mechanical properties: assessment model. *Int J Geomech* 19(7):06019012
- Zhang FY, Kong R, Peng JB (2018) Effects of heating on compositional, structural, and physicochemical properties of loess under laboratory conditions. *Appl Clay Sci* 152:259–266
- Zhang HC, Zhang LY, Mahancy WC (1991) Element geochemistry of the jiuzhoutai loess section. *Lanzhou Geochim* 1:79–86 (In Chinese)
- Zhang N, Liu X, Lan H (2021) Characterizing saturation state of loess using p-wave velocity. *Eng Geol* 290(30):106207
- Zhang WX, Shi ZT, Chen GJ, Liu Y, Niu J, Ming QZ, Huai Su (2013) Geochemical characteristics and environmental significance of Taledo loess-paleosol sequences of Ili Basin in Central Asia. *Environ Earth Sci* 70:2191–2202
- Zhang ZG (1980) Loess in China. *GeoJournal* 4(6):525–540
- Zhu J, Su Z, Zhang H (2022) Soil–water characteristic curves and hydraulic conductivity of Gaomiaozi bentonite pellet-contained materials. *Environ Earth Sci* 81(3):92
- Zhu J, Zhang H, Wang Z, Yang S, Ding Z (2021) Physico-mechanical properties of thick paleosol in Q₁ strata of the Chinese Loess Plateau and their variations during tunnel excavation. *Eng Geol* 295:106426
- Zhuang JQ, Peng JB, Wang GH, Javed I, Wang Y, Lia W (2018) Distribution and characteristics of landslide in Loess Plateau: A case study in Shaanxi province. *Eng Geol* 236:89–96

Publisher's Note Springer Nature remains neutral with regard to jurisdictional claims in published maps and institutional affiliations.

Springer Nature or its licensor holds exclusive rights to this article under a publishing agreement with the author(s) or other rightsholder(s); author self-archiving of the accepted manuscript version of this article is solely governed by the terms of such publishing agreement and applicable law.